

Citation:
Cheung, C, Yeoh, G and Tu, J 2007, 'On the numerical study of isothermal vertical bubbly flow using two population balance approaches', *Chemical Engineering Science*, vol. 62, no. 17, pp. 4659-4674.

On the numerical study of isothermal vertical bubbly flow using two population balance approaches

Sherman C.P. Cheung¹, G.H. Yeoh² and J.Y. Tu¹

¹*School of Aerospace, Mechanical and Manufacturing Engineering, RMIT University,
Victoria 3083, Australia*

²*Australian Nuclear Science and Technology Organisation (ANSTO), PMB 1, Menai,
NSW 2234, Australia*

Revised Manuscript

Corresponding Author : Prof. Jiyuan Tu
SAMME,
RMIT University, Bundoora,
Melbourne, Victoria 3083, Australia

Email : jiyuan.tu@rmit.edu.au

Phone no. : +61-3-9925 6191

Fax no. : +61-3-9925 6108

Submitted to: Chemical Engineering Science
Submission Date: 4th April 2007

Abstract

Two population balance approaches based on the Multiple-Size-Group (MUSIG) model and one-group Average Bubble Number Density (ABND) model for handling the bubble size distribution of gas-liquid bubbly flows under isothermal conditions are assessed. Three forms of coalescence and breakage mechanisms by Wu et al. (1998), Hibiki and Ishii (2002) and Yao and Morel (2004) are incorporated in the ABND model. To examine the relative merits of both approaches, local radial distributions of five primitive variables in bubbly flows: void fraction, Sauter mean bubble diameter, interfacial area concentration, and gas and liquid velocities, are compared against the experimental data of Liu and Bankoff (1993a,b) and Hibiki et al. (2001). In general, both of the ABND model and MUSIG model predictions yield close agreement with experimental results. To account for the range of different bubble sizes in the gas-liquid bubbly flows, the resolution required is achieved through the application of the MUSIG model. Nevertheless, computational times increase by a factor of two when compared to applying the simpler ABND model. To further exploit the models' capabilities, investigations are carried out by extending the two population approaches beyond the bubbly flow regime of higher void fraction, particularly in the transition regime. The numerical results are found to be grossly over-predicted, which expose the inherent limitations of the models. It is known that bubbles in this regime are generally highly distorted and closely packed instead of spherically shape and allowed to move freely in bubbly flow regime.

Keywords: Population balance; bubbly flow; CFD; average bubble number density

Nomenclature

a_{if}	Interfacial area concentration
c_f	increase coefficient of surface area
C	Adjustable model constant
C_D	Drag coefficient
C_L	Lift coefficient
C_{RC}	Random collision coefficient
C_{TD}	Turbulent dispersion coefficient
C_{TI}	Turbulent impact coefficient
C_{w1}, C_{w2}	Wall lubrication constants
C_{WE}	Wake entrainment coefficient
d	parent bubble diameter
d_i, d_j	daughter bubble diameters
d_H	Maximum bubble horizontal dimension
D	Inner diameter of the pipe
D_B	death rate due to break-up
D_C	death rate due to coalescence
D_s	Sauter mean bubble diameter
EO	Eötvös number
EO_{dg}	Modified Eötvös number
f_{BV}	breakage volume fraction
f_i	scalar variable of the dispersed phase
F_C, F_B	Coalescence and Breakage calibration factors
F_{lg}	Total interfacial force
F_{lg}^{drag}	Drag force
F_{lg}^{lift}	Lift force
$F_{lg}^{\text{lubrication}}$	Wall lubrication force
$F_{lg}^{\text{dispersion}}$	Turbulent dispersion force
IAC	Interfacial area concentration
g	Gravitational acceleration
\vec{g}	Gravitational vector
h_0	initial film thickness
h_f	critical film thickness
k	Turbulent kinetic energy
\vec{n}_w	Outward vector normal to the wall surface
n	Average number density of gas phase (bubble)

n_i	number density of the i th class
n_j	number density of the j th class
P	Pressure
P_B	production rate due to break-up
P_C	production rate due to coalescence
Re	Flow Reynolds number
R_j	Net change rate of number density due to coalescence and break-up
t	Physical time
u	Velocity
u_t	Turbulent Velocity
\bar{u}	Velocity vector
U	relative velocity between gas and liquid phase
U_r	terminal velocity of bubbles
v_i, v_j	volume corresponding to bubble group i and j
We	Weber number
We_{cr}	Critical Weber number
y_w	Adjacent point normal to the wall surface

Greek Symbols

α	Void fraction
α_{max}	Maximum allowable void fraction
ε	Turbulence kinetic energy dissipation
η_{jki}	transfer coefficient between bubble groups arising from bubble breakup
λ	Eddy size in the inertial subrange
μ^e	Effective viscosity
$\nu_{t,g}$	Turbulent kinematic viscosity
ξ	size ratio between an eddy and a particle in the inertial subrange
ρ	Density
$\Delta\rho$	Density difference = $\rho_l - \rho_g$
σ	Surface tension
$\sigma_{t,g}$	Turbulent Schmidt number
τ_{ij}	Bubble contact time
ϕ_n^{RC}	Bubble number density change rate due to random collision
ϕ_n^{TI}	Bubble number density changes rate due to impact of turbulent eddies
$\phi_n'^{RC}$	Modified random collision rate
$\phi_n'^{TI}$	Modified turbulent induced breakage rate
ϕ_n^{WE}	Bubble number density changes rate due to wake entrainment
χ_{ij}	Turbulent random coalescence rate
$\Omega(v)$	Bubble breakup rate

Subscripts

g	Gas
gl	Transfer of quantities from liquid phase to vapour phase
i	Index of gas/liquid phase
l	Liquid
lg	Transfer of quantities from gas phase to liquid phase
min	Minimum operator
max	Maximum operator

1 Introduction

Bubble column reactors, extensively used in a various chemical, petroleum, mining, food and pharmaceutical industries, are usually known as excellent systems for processes that require large interfacial areas for gas-liquid mass transfer and efficient mixing for competing gas-liquid reactions. Productivity of such kind of reactor is nonetheless governed by the limitations imposed by the interfacial areas that are affected by various hydrodynamic aspects such as the bubble size distribution as well as bubble coalescence and break-up rates. To better optimise bubble column design, a greater reliance on the fundamental knowledge of population balance of bubbles is required.

Population balance modelling is becoming ever more prevalent in many industrial applications. The use of population balance in any system is to account for a record of the number of entities existing within the system, which for bubbly flow are bubbles, whose presence or occurrence may govern the behaviour of the system under consideration. In most of this system, the record of these entities is dynamically changing depending on the “birth” and “death” processes that create and destroy entities through the state space. The mechanistic behaviours of coalescence and breakage of bubbles in bubbly flows are examples of such processes.

The foundation development of the population balance equation stems from the consideration of the Boltzman equation, where such an equation is generally expressed as an integrodifferential form of the particle distribution function. Owing to the complex phenomenological nature of events, analytical solutions are only available in very few cases (Bove et al., 2005). Nevertheless, mounting interest on population balances have resulted in several existing and emerging numerical techniques for solving the population balance equations (PBEs): Monte Carlo method (Ramkrishna, 2000), the

method of discrete classes (Kumar and Ramkrishna, 1996a,b), the quadrature method of moments (Marchisio et al., 2003a,b), the direct quadrature method of moments (Marchisio and Fox, 2005) and the least square method (Dorao and Jakobsen, 2006, 2007). Among the many available numerical techniques, the method of discrete classes has received particular interest due to its rather straightforward implementation within CFD program. This method nonetheless suffers from discretization errors, which may bring to question the reliability of the model predictions. It will be demonstrated later that the main source of prediction error for gas-liquid flows comes predominantly from the spherical bubble assumption taken into account for the coalescence and break-up kernels and the uncertainties embedded in turbulence modelling. The method of discrete class is therefore adopted in the present study.

With encouraging results demonstrated through a number of research studies, the population balance concept has been considered as a promising future modelling direction (Ramkrishna and Mahoney, 2002). Several studies based on the Multiple-Size-Group (MUSIG) model by Pochorecki et al. (2001), Olmos et al. (2001), Yeoh and Tu (2004), Frank et al., (2005), and Yeoh and Tu (2005) typified the application of this particular category of population balance approach. In the method of discrete classes, the continuous size range of bubbles is discretized into a number of discrete size classes. For each class, a scalar (number density of bubbles) equation is solved to accommodate the population changes caused by intra/inter-group bubble coalescence and break-up. However, excessive computational calculations to solve a large number of bubble classes for some gas-liquid flows having a wide range of bubble size distribution may significantly overwrite the potential benefits of the MUSIG model originally aims to achieve (Bove et al., 2005).

Alternatively, a transport equation for the interfacial area has been developed by a number of researchers (Kocamustafaogullari and Ishii, 1995; Wu et al, 1998; Hibiki and Ishii, 2002; Yao and Morel, 2004). Similar to the formulation of the interfacial area transport equation, an Average Bubble Number Density (ABND) equation was proposed very recently in our previous studies (Yeoh and Tu, 2006; Cheung et al., 2006). As the distribution of bubbles is now represented by a single average scalar (i.e. interfacial area or bubble number density) in the formulations, these average scalar transport equations can be regarded as another simpler form for solving the population balance of bubbles. Chen et al. (2005) argued that the assumption of “mean” bubble size is only justified in bubbly flow where the range of bubble size is considerably narrow. For the bubbly flows considered, the application of the ABND is assessed against the use of a more sophisticated approach of the MUSIG model.

Based on our previous work (Yeoh and Tu, 2006; Cheung et al., 2006), the primary aim of this paper is to determine the relative merits and capabilities applying two population balance approaches (i.e. MUSIG and ABND models) within the CFD framework to resolve various isothermal bubbly and bubbly-to-slug transition flow conditions. Particular attention is directed towards how these two different approaches measure up in handling bubbly-to-slug transition flow conditions. Three coalescence and break-up mechanism specifically by Wu et al. (1998), Hibiki and Ishii (2002) and Yao and Morel (2004) are incorporated in the ABND model. Predictions by the ABND and MUSIG models are compared against two different experimental data of isothermal gas-liquid bubbly flow in a vertical pipe performed by Liu and Bankoff (1993a, 1993b) and Hibiki et al. (2001).

2 Mathematical Models

2.1 Two-Fluid model

2.1.1 Mass conservation

Numerical simulations presented in this paper are based on the two-fluid model Eulerian-Eulerian approach. The liquid phase is treated as continuum while the gas phase (bubbles) is considered as dispersed phase (ANSYS, 2005). In isothermal flow condition, with no interfacial mass transfer, the continuity equation of the two-phases with reference to Ishii (1975) and Drew and Lahey (1979) can be written as:

$$\frac{\partial(\rho_i \alpha_i)}{\partial t} + \nabla \cdot (\rho_i \alpha_i \bar{u}_i) = 0 \quad (1)$$

where α , ρ and \bar{u} is the void fraction, density and velocity of each phase. The subscripts $i = l$ or g denotes the liquid or gas phase.

2.1.2 Momentum conservation

The momentum equation for the two-phase can be expressed as follow:

$$\frac{\partial(\rho_i \alpha_i \bar{u}_i)}{\partial t} + \nabla \cdot (\rho_i \alpha_i \bar{u}_i \bar{u}_i) = -\alpha_i \nabla P + \alpha_i \rho_i \bar{g} + \nabla \cdot [\alpha_i \mu_i^e (\nabla \bar{u}_i + (\nabla \bar{u}_i)^T)] + F_i \quad (2)$$

On the right hand side of Eq. (2), F_i represents the total interfacial force calculated with averaged variables, \bar{g} is the gravity acceleration vector and P is the pressure. From the above equation, it is noted that closure law is required to determine the momentum transfer of the total interfacial force. This force strongly governs the distribution of the liquid and gas phases within the flow volume. Details of the closure are given below.

2.2 Interfacial momentum transfer

In isothermal bubbly flows, as demonstrated by Frank et al. (2004), interfacial momentum transfer exhibits a dominant effect in the multiphase momentum equations.

The total interfacial forces considered in the present study can be categorized into four main terms: drag, lift, lubrication and turbulence dispersion:

$$F_i = F_{lg} = -F_{gl} = F_{lg}^{\text{drag}} + F_{lg}^{\text{lift}} + F_{lg}^{\text{lubrication}} + F_{lg}^{\text{dispersion}} \quad (3)$$

Here, F_{lg} denotes the momentum transfer terms from the gas phase to the liquid phase and vice versa for F_{gl} .

2.2.1 Drag force

The inter-phase momentum transfer between gas and liquid due to the drag force resulted from shear and form drag is modelled according to Ishii and Zuber (1979) as:

$$F_{lg}^{\text{drag}} = -F_{gl}^{\text{drag}} = \frac{1}{8} C_D a_{if} \rho_l |\bar{u}_g - \bar{u}_l| (\bar{u}_g - \bar{u}_l) \quad (4)$$

where C_D is the drag coefficient which can be evaluated by correlation of several distinct Reynolds number regions for individual bubbles proposed by Ishii and Zuber (1979).

2.2.2 Lift force

Due to velocity gradients in radial and azimuthal directions, bubbles rising in a liquid are subjected to a lateral lift force. The force can be correlated to the relative velocity and the local liquid vorticity from Drew and Lahey (1979) as:

$$F_{lg}^{\text{lift}} = -F_{gl}^{\text{lift}} = C_L \rho_l (\bar{u}_g - \bar{u}_l) \times (\nabla \times \bar{u}_l) \quad (5)$$

For the lift coefficient, C_L , the Eötvös number dependent correlation proposed by Tomiyama (1998) is adopted and the lift coefficient can then be expressed as:

$$C_L = \begin{cases} \min[0.288 \tanh(0.121 \text{Re}_g); f(Eo_{dg})] & Eo_g < 4 \\ f(Eo_{dg}) = 0.00105 Eo_{dg}^3 - 0.0159 Eo_{dg}^2 - 0.0204 Eo_{dg} + 0.474 & 4 \leq Eo_g \leq 10 \\ -0.29 & Eo_g > 10 \end{cases} \quad (6)$$

where Re_g is the local Reynolds number of the gas phase (bubbles) and Eo_g is the Eötvös number. The modified Eötvös number of the gas phase is:

$$Eo_{dg} = \frac{g(\rho_l - \rho_g)d_H^2}{\sigma} \quad (7)$$

The variable d_H is the maximum bubble horizontal dimension that can be evaluated by using the empirical correlation of Wellek et al. (1966):

$$d_H = D_s(1 + 0.163Eo_g^{0.757})^{1/3} \quad (8)$$

2.2.3 Wall lubrication force

In contrast to the lift force, lateral force due to the surface tension is formed to prevent bubbles attaching on the solid walls thereby results in a low gas void fraction at the vicinity of the wall area. The force is well-known as wall lubrication force which can be modelled according to Antal et al. (1991) given by:

$$F_{lg}^{\text{lubrication}} = -F_{gl}^{\text{lubrication}} = -\left(C_{w1} + C_{w2} \frac{D_s}{y_w}\right) \frac{\alpha_g \rho_l [(\bar{u}_g - \bar{u}_l) - ((\bar{u}_g - \bar{u}_l) \cdot \bar{n}_w) \bar{n}_w]^2}{D_s} \quad (9)$$

where y_w is the distance from the wall boundary and \bar{n}_w is the outward vector normal to the wall. Following the proposal by Krepper et al. (2005), the model constants are $C_{w1} = -0.0064$ and $C_{w2} = 0.016$. Moreover, for avoiding attraction force emerges,

the force is set to zero if the wall distance satisfies the follow condition: $y_w > \frac{C_{w2}}{C_{w1}} D_s$.

2.2.4 Turbulent dispersion force

In the consideration of turbulence assisted bubble dispersion, the turbulent dispersion force expression in terms of Farve-averaged variables proposed by Burns et al. (2004) is adopted, viz:

$$F_{lg}^{\text{dispersion}} = -F_{gl}^{\text{dispersion}} = C_{TD} C_D \frac{v_{t,g}}{\sigma_{t,g}} \left(\frac{\nabla \alpha_l}{\alpha_l} - \frac{\nabla \alpha_g}{\alpha_g} \right) \quad (10)$$

with C_{TD} , C_D , $v_{t,g}$ and $\sigma_{t,g}$ is the turbulent dispersion coefficient, drag force coefficient, turbulent kinematic viscosity for the gas phase and the turbulent Schmidt

number of the gas phase respectively. By default, the turbulent dispersion coefficient $C_{TD} = 1$ and the turbulent Schmidt number $\sigma_{t,g} = 0.9$ is adopted.

2.3 Average Bubble Number Density (ABND) transport equation

For the dispersed isothermal bubbly flow without the consideration of mass transfer due to evaporation and condensation, the population balance of dispersed bubbles is mainly governed by three mechanisms of bubble coalescence and breakage, which can be expressed in the following average bubble number density transport equation:

$$\frac{\partial n}{\partial t} + \nabla \cdot (\bar{u}_g n) = \phi_n^{RC} + \phi_n^{TI} + \phi_n^{WE} \quad (11)$$

where n is the average bubble number density; ϕ_n^{RC} , ϕ_n^{TI} and ϕ_n^{WE} are the bubble number density changes due to random collision, turbulent induced breakage and wake entrainment. With the assumption of spherical bubbles, using algebraic substitution, the above transport equation is equivalent to the interfacial area transport equation which has been derived by Hibiki and Ishii (2000a). The phenomenological mechanism of coalescence and breakage source terms need closure to describe the spatial evolution of the gas phase. Three models describing the coalescence and breakage effects are employed in the present study. Formulation of each model is briefly discussed below.

2.3.1 Wu et al. (1998) Model

An empirical modelling of the bubble coalescence and bubble breakage that has been widely cited is the model developed by Wu et al. (1998). Considering the characteristic times for binary collision and the mean travelling length between neighbouring bubbles, they have modelled the random collision rate of bubble coalescence according to:

$$\phi_n^{RC} = -C_{RC} \frac{\alpha_g^2 \varepsilon^{1/3}}{D_S^{11/3} \alpha_{max}^{1/3} (\alpha_{max}^{1/3} - \alpha_g^{1/3})} \left[1 - \exp\left(-\frac{C \alpha_{max}^{1/3} \alpha_g^{1/3}}{\alpha_{max}^{1/3} - \alpha_g^{1/3}}\right) \right] \quad (12)$$

where $C_{RC} = 0.021$ and $C = 3.0$ are the adjustable model constants representing the coalescence efficiency. The maximum allowable void fraction $\alpha_{max} = 0.8$ was chosen considering the transition point from slug to annular flow.

Assuming a spherical bubble travelling with its terminal velocity, the rate of collision caused by wake entrainment is expressed as:

$$\phi_n^{WE} = -C_{WE} U_r \frac{\alpha_g^2}{D_S^4} \quad (13)$$

where $C_{WE} = 0.0073$ is a model constant determining the effective wake length and the coalescence efficiency. The terminal velocity of bubbles, U_r , is given by:

$$U_r = \left(\frac{D_S g \Delta \rho}{3 C_D \rho_l} \right)^{1/2} \quad (14)$$

Turbulent induced breakage is derived from a simple momentum balance approach. In this mechanism, Wu et al. (1998) restricted only eddies with the same size as the bubbles responsible for breakage. The rate of bubble is given by:

$$\phi_n^{TI} = C_{TI} \frac{\alpha_g \varepsilon^{1/3}}{D_S^{11/3}} \left(1 - \frac{We_{cr}}{We} \right) \exp \left(- \frac{We_{cr}}{We} \right) \quad (15)$$

Here, $C_{TI} = 0.0945$ while the critical Weber number $We_{cr} = 2.0$ governs the criterion of breakage, are adjustable parameters.

2.3.2 Hibiki and Ishii (2002) Model

In contrast to the model of Wu et al. (1998), Hibiki and Ishii (2002) ignored the wake entrainment coalescence due to its insignificant effect in bubbly flow condition. By assuming bubble movement behaves analogously to ideal gas molecules, the coalescence rate due to turbulent random collision is determined as:

$$\phi_n^{RC} = -C_{RC} \frac{\alpha_g^2 \varepsilon^{1/3}}{D_S^{11/3} (\alpha_{max} - \alpha_g)} \exp \left(- C \frac{\rho_l^{1/2} \varepsilon^{1/3} D_S^{5/6}}{\sigma^{1/2}} \right) \quad (16)$$

Instead of using a constant in Wu et al. (1998) model, coalescence efficiency is derived from the liquid-film-thinning model (Oolman and Blanch, 1986a, 1986b) and dimensional consideration for turbulent flow (Levich, 1962) using the Coualaloglou and Tavlarides (1977) expression as the main framework. $C_{RC} = 0.03$ and $C = 1.29$ are the adjustable model constants that have been calibrated through experiments. Furthermore, Hibiki and Ishii (2000a) also derived the breakage rate from kinetic theory. The breakage rate is correlated to the frequency for a given bubble colliding with the turbulent eddy as:

$$\phi_n^{TI} = C_{TI} \frac{\alpha_g^2 (1 - \alpha_g) \varepsilon^{1/3}}{D_S^{11/3} (\alpha_{\max} - \alpha_g)} \exp\left(-C \frac{\sigma}{\rho_l \varepsilon^{2/3} D_S^{5/3}}\right) \quad (17)$$

Here, $C_{TI} = 0.03$ and $C = 1.37$ are also adjustable model constants determined experimentally.

2.3.3 Yao and Morel (2004) Model

Recently, Yao and Morel (2004) pointed out that the aforementioned two models were developed based on two different considerations: the free travelling time or the interaction time. They argued that both characteristic times are identically important. Taking two considerations into account, the bubbles coalescence rate is derived as:

$$\phi_n^{RC} = -C_{RC1} \frac{\alpha_g^2 \varepsilon^{1/3}}{D_S^{11/3}} \frac{\exp(-C_{RC2} \sqrt{We/We_{cr}})}{(\alpha_{\max}^{1/3} - \alpha_g)/\alpha_{\max}^{1/3} + C_{RC3} \alpha_g \sqrt{We/We_{cr}}} \quad (18)$$

where the derived coefficients are respectively $C_{RC1} = 2.86$, $C_{RC2} = 1.017$ and $C_{RC3} = 1.922$. Similar to the Hibiki and Ishii (2002) model, coalescence caused by wake entrainment is neglected.

For the bubble breakage, they disputed that bubble breakage is mainly caused by the resonance oscillation. Considering the natural frequency of the oscillating bubbles, the interaction time can be approximated and the rate of bubble breakage is given by:

$$\phi_n^{TI} = C_{TI1} \frac{\alpha_g (1 - \alpha_g) \varepsilon^{1/3}}{D_S^{11/3}} \frac{\exp(-We_{cr}/We)}{1 + C_{TI2} (1 - \alpha_g) \sqrt{We/We_{cr}}} \quad (19)$$

where the coefficients are respectively $C_{TI1} = 1.6$ and $C_{TI2} = 0.42$. The critical Weber number of 1.42 was employed (Sevik and Park, 1973). Considering the transition point between the finely dispersed bubbly and slug flows, the maximum allowable void fraction in Hibiki and Ishii (2002) and Yao and Morel (2004) models retains a value of 0.52.

2.4 MUSIG Model

To account for non-uniform bubble size distribution, the MUSIG model employs multiple discrete bubble size groups to represent the population balance of bubbles. Assuming each bubble class travel at the same mean algebraic velocity, individual number density of bubble class i based on Kumar and Ramkrishna (1996a) can be expressed as:

$$\frac{\partial n_i}{\partial t} + \nabla \cdot (\bar{u}_g n_i) = \left(\sum_j R_j \right)_i \quad (20)$$

where $\left(\sum_j R_j \right)_i$ represents the net change in the number density distribution due to coalescence and break-up processes. The discrete bubble class between bubble volumes v_i and v_{i+1} is represented by the centre point of a fixed non-uniform volume distributed grid interval. Similar to Eq. (11), the interaction term $\left(\sum_j R_j \right)_i = (P_C + P_B - D_C - D_B)$ contains the source rate of P_C , P_B , D_C and D_B , which are, respectively, the production rates due to coalescence and break-up and the death rate due to coalescence and break-up of bubbles.

2.4.1 MUSIG Break-up rate

The production and death rate of bubbles due to the turbulent induced breakage is formulated as:

$$P_B = \sum_{j=i+1}^N \Omega(v_j : v_i) n_j$$

$$D_B = \Omega_i n_i \quad \text{with} \quad \Omega_i = \sum_{k=1}^N \Omega_{ki} \quad (21)$$

Here, the break-up rate of bubbles of volume v_j into volume v_i is modelled according to the model developed by Luo and Svendsen (1996). Similar to the aforementioned ABND models, the model is developed based on the assumption of bubble binary break-up under isotropic turbulence situation. The major different is the daughter size distribution have been taken account using a stochastic breakage volume fraction f_{BV} . By incorporating the increase coefficient of surface area, $c_f = [f_{BV}^{2/3} + (1-f_{BV})^{2/3} - 1]$, into the breakage efficient, the break-up rate of bubbles can be obtained as:

$$\frac{\Omega(v_j : v_i)}{(1-\alpha_g) n_j} = F_B C \left(\frac{\varepsilon}{d_j^2} \right)^{1/3} \int_{\xi_{min}}^1 \frac{(1+\xi)^2}{\xi^{11/3}} \times \exp\left(-\frac{12c_f \sigma}{\beta \rho_l \varepsilon^{2/3} d^{5/3} \xi^{11/3}} \right) d\xi \quad (22)$$

where $\xi = \lambda / d_j$ is the size ratio between an eddy and a particle in the inertial sub-range and consequently $\xi_{min} = \lambda_{min} / d_j$ and C and β are determined, respectively, from fundamental consideration of drops or bubbles breakage in turbulent dispersion systems to be 0.923 and 2.0. F_B is the breakage calibration factor which will be discussed later.

2.4.2 MUSIG Coalescence rate

The number density of individual bubble groups governed by coalescence can be expressed as:

$$\begin{aligned}
P_C &= \frac{1}{2} \sum_{k=1}^i \sum_{l=1}^i \eta_{jki} \chi_{ij} n_i n_j \\
\eta_{jki} &= \begin{cases} (v_j + v_k) - v_{i-1} / (v_i - v_{i-1}) & \text{if } v_{i-1} < v_j + v_k < v_i \\ v_{i+1} - (v_j + v_k) / (v_{i+1} - v_i) & \text{if } v_i < v_j + v_k < v_{i+1} \\ 0 & \text{otherwise} \end{cases} \\
D_C &= \sum_{j=1}^N \chi_{ij} n_i n_j \tag{23}
\end{aligned}$$

As discussed in the previous section, bubble coalescence occurs via collision of two bubbles which may be caused by wake entrainment, random turbulence and buoyancy. However, only turbulence random collision is considered in the present study as all bubbles are assumed to be spherical (wake entrainment becomes negligible). Furthermore, as all bubbles travel at the same velocity in the MUSIG model, buoyancy effect is also eliminated. The coalescence rate considering turbulent collision taken from Prince and Blanch (1990) can be expressed as:

$$\chi_{ij} = F_C \frac{\pi}{4} [d_i + d_j]^2 (u_i^2 + u_j^2)^{0.5} \exp\left(-\frac{t_{ij}}{\tau_{ij}}\right) \tag{24}$$

where τ_{ij} is the contact time for two bubbles given by $(d_{ij}/2)^{2/3} / \varepsilon^{1/3}$ and t_{ij} is the time required for two bubbles to coalesce having diameter d_i and d_j estimated to be $[(d_{ij}/2)^3 \rho_l / 16\sigma]^{0.5} \ln(h_0 / h_f)$. The equivalent diameter d_{ij} is calculated as suggested by Chesters and Hoffman (1982): $(d_{ij} = (2/d_i + 2/d_j)^{-1})$. According to Prince and Blanch (1990), for air-water systems, experiments have determined the initial film thickness h_0 and critical film thickness h_f at which rupture occurs as 1×10^{-4} and 1×10^{-8} m respectively. The turbulent velocity u_t in the inertial subrange of isotropic turbulence (Rotta, 1972) is given by: $u_t = \sqrt{2\varepsilon^{1/3} d^{1/3}}$. Again, F_C is the coalescence calibration factor which will be discussed section 5. In the present study, bubbles ranging from 0 mm to 10 mm diameter are equally divided into 10 size groups (see Table 3).

3 Experimental details

The experimental set-up of Liu and Bankoff (1993a, 1993b) consisted of a test section with 2800mm long and a vertical acrylic pipe with an internal diameter of $D = 38$ mm. Distilled water was circulated within the testing loop by a centrifugal pump and temperature was maintained in the range of $10 \pm 0.01^\circ\text{C}$ by cooling coils and heater installed in the water tank. Bubbles were produced and injected into the test section via a bundle of 64 equally-spaced 0.1 mm hypodermic needles at the bottom. Local radial measurements were obtained at the axial location of $z/D = 36.0$. Liquid velocity was attained by using hot-film anemometers while local void fraction and gas velocity were measured with two-point resistivity probe. A total of 48 flow conditions which covered the range j_g : 0.027-0.347 m/s and j_f : 0.376-1.391 m/s was investigated. The bubble diameters were controlled in a narrow range of 2-4 mm during the whole course of the experiments.

Similar to the set-up of Liu and Bankoff (1993a), the experimental data by Hibiki et al. (2001) was taken in an acrylic round pipe with an inner diameter $D = 50.8\text{mm}$ and a length of 3061 mm. The temperature of the apparatus was kept at a constant temperature (i.e. 20°C) within a deviation of $\pm 0.2^\circ\text{C}$ by a heat exchanger installed in a water reservoir. Local flow measurements using the double sensor and hotfilm anemometer probes were performed at three axial (height) locations of $z/D=6.0$, 30.3 and 53.5 and 15 radial locations of $r/R=0$ to 0.95. Experiments at a range of superficial liquid velocities j_f and superficial gas velocities j_g were performed, which covered most of the bubbly flow regions, including finely dispersed bubbly flow and bubbly-to-slug transition flow regions.

The aforementioned coalescence/coalescence/breakage models for the ABND and MUSIG approaches have been primarily developed under bubbly flow conditions.

Bubbles were idealized according to spherical shape and finely dispersed bubbles were assumed to occupy the entire two-phase fluid flow domain. The primary objective in this present study is to compare the two population balance approaches for simulating bubbly flow regime. The experimental dataset of Liu and Bankoff (1993a) and Hibiki et al. (2001) in bubbly flow regime have been selected for validating these models. Six flow conditions were studied as depicted in Fig. 1. Also included in the figure, the solid lines represented the different flow regime transition boundaries predicted by the model of Taitel et al. (1980). As shown in the figure, all the six flow conditions lie within the bubbly flow region. As will be demonstrated later, these models were also assessed for their possible applications at high gas superficial velocity (i.e. transition regime). Two transition flow condition of Hibiki et al. (2001) were used (see also in Fig. 1). Details of the flow conditions are summarized in Table 1. For ease of discussion, experiments by Liu and Bankoff (1993a) and Hibiki et al. (2001) are hereafter referred as Exp. 1 and Exp. 2 respectively.

4 Numerical Details

In modelling isothermal gas-liquid bubbly flow, two sets of governing equations for momentum were solved. The generic CFD code ANSYS CFX 10 (ANSYS, 2005) was employed as a platform for two-fluid flow computation. The average bubble number density transport equation with appropriate sink or source terms describing the coalescence and break-up rate of bubble was also implemented through the CFX Command Language (CCL). The built-in MUSIG model was adopted for MUSIG simulations. Radial symmetry has been used in simulations. Numerical simulations were performed on a 60° radial sector of the pipe with symmetry boundary conditions at both vertical sides. At the inlet of the test section, as the diameter of the injected bubbles are unknown, uniformly distributed superficial liquid and gas velocities, void

fraction and bubble size were specified in accordance with the flow condition described. Details of the boundary conditions have been also summarized in Table 1. At the pipe outlet, a relative averaged static pressure of zero was specified. Fig. 2 shows the mesh distribution within the computational model. For all flow conditions, reliable convergence were achieved within 2500 iterations when the RMS (root mean square) pressure residual dropped below 1.0×10^{-7} . A fixed physical time scale of 0.002s is adopted for all steady state simulations.

In handling bubble induced turbulent flow, unlike single phase fluid flow problem, no standard turbulence model is tailored for two-phase (liquid-air) flow. Nevertheless, numerical investigation revealed that standard $k-\varepsilon$ model predicted an unrealistically high gas void fraction peak close to wall (Frank et al., 2004, Cheung et al., 2006). The $k-\omega$ based Shear Stress Transport (SST) model by Menter (1994) provided more realistic prediction of void fraction close to wall.

The SST model is a hybrid version of the $k-\varepsilon$ and $k-\omega$ models with a specific blending function. Instead of using empirical wall function to bridge the wall and the far-away turbulent flow, the $k-\omega$ model solves the two turbulence scalars right up to the wall boundary. This approach eliminates errors arising from empirical wall function and thus provides better prediction at the near wall region. It is thereby not surprise that more accurate liquid or gas velocities can be captured by the SST model which eventually provides better predictions of void fraction close to wall. The SST model is thereby employed in the present study. Moreover, to account for the effect of bubbles on liquid turbulence, the Sato's bubble-induced turbulent viscosity model (Sato et al., 1981) has been adopted as well.

A three-dimensional mesh containing hexagonal elements was generated over the entire pipe domain. Six mesh structures corresponding to coarse, medium and fine with

three different mesh levels were tested covering the range of 4,000-69,120 elements for Exp. 1 and 4,000-108,100 elements for Exp. 2 (see Table 2). Comparing the predicted results between the medium and fine mesh, small discrepancies were observed. The maximum differences between these two mesh levels in the two experimental flow conditions were less than 5%. It can therefore be concluded that the fine mesh level is sufficient for obtaining grid independent solutions. Hereafter, predicted results shown were all obtained from the fine mesh.

5 Results and Discussion

Based on the experiments performed by Hibiki et al. (2001), they have observed that there was insignificant development of the Sauter mean bubble diameter along the axial direction. From the phenomenological view point, this implied that the breakage and coalescence rate among bubbles attained near equilibrium condition. Analogous findings have also been reported from other experimentalists (Bukur et al., 1996; George et al., 2000). In our numerical simulations, coalescence rate was nonetheless found to be around 10 and 20 times higher than breakage rate in ABND and MUSIG model respectively. Recently, similar difficulty in simulating bubble columns flows has been also reported by Chen et al. (2005). Coalescence rate was found about one order of magnitude higher than the breakage rate in their work. A plausible explanation for this discrepancy could be attributed to the error embedded in the turbulent dissipation rate prediction (Bertola et al., 2003).

For engineering estimation and maintaining the balance of the coalescence and breakage terms, Chen et al. (2005) enhanced the breakage rates by a factor of 10 in their calculations. Similarly, in the work by Olmos et al. (2001), calibration factor of 0.075 was also employed. In the present study, follow the same argument, the coalescence rate has been reduced by a factor of 1/10 in the ABND model (i.e. $\phi_n^{*TI} = \phi_n^{TI}$, $\phi_n^{*RC} = 0.1\phi_n^{RC}$).

Similarly, for the MUSIG model, coalescence and breakage calibration factors (i.e. F_C and F_B), were set as 0.05 and 1.0 respectively. It should be emphasised that the reduction and calibration factors are introduced by the mere means for engineering estimation, which may be case sensitivity and subject to the flow condition. Although adjustment to the reduction factor could obtain “better” results, it loses, however, the predictive nature of the models and the common ground for comparison. Therefore, values of the reduction and calibration factors are fixed for all the cases and flow conditions studied in this work.

5.1 *Experimental data of Liu and Bankoff (1993a, 1993b)*

5.1.1 *Void fraction distribution*

Fig. 3 shows the void fraction distributions obtained from the MUSIG model and the three coalescence/breakage mechanisms employed in the ABND model comparing with the measured data at the dimensionless axial position $z/D=36.0$. From the phenomenological view point, the phase distribution patterns along the radial direction of the bubble column exhibits four basic types of distributions: “wall peak”, “intermediate peak”, “core peak” and “transition”, as categorized by Serizawa and Kataoka (1988).

In the bubbly flow regime, maximum void fraction located close to the wall demonstrated the flow phase distributions typically known as the “wall peak” behaviour, which was mainly due to the positive lift force pushing the small bubbles toward the pipe wall. As depicted in Fig. 3, a well-developed wall peaking behaviour was recorded in the experiment and had been successfully captured by the ABND and MUSIG models. In the case of low gas superficial velocity (i.e. $[\alpha_g] = 2.5\%$, see also in Fig. 3a), all models of ABND approach under-estimated the void fraction at the core of

the pipe. In contrast, MUSIG model provided closer predictions with the experiment. However, as shown in Fig. 3b, void fractions at the core of the high gas superficial velocity case were slightly over-predicted by all models. One of the possible reasons of the over-prediction of the void fraction distribution could be the uncertainties associated with the application of the turbulence model for two-phase flow which inadequately predicted the turbulent energy dissipation and eventually affected the bubbles coalescence/breakage rate.

As also pointed out by Frank et al. (2004), predicted wall lubrication forces of the Antal et al. (1991) model were generally relatively weak when compared with the other two models by Frank et al. (2004) and Tomiyama (1998). Applying these latter models might yield much larger values; the maximum radial gas fraction might be now found at some considerable distance away from the wall as recorded in the experiments. The adopted Antal et al. (1991) model could thus be another source of error causing the overestimated void fraction at the wall. In general, as similar assumptions and hypothesis have been adopted in the ABND and MUSIG models, predicted void fraction profiles are considerably similar while MUSIG model tends to provide higher void fraction values at the core region.

5.1.2 Time-averaged liquid velocity

The measured and predicted radial profiles of the liquid velocity are shown in Fig. 4. In contrast to single phase flow, the introduction of bubbles into the liquid flow has the tendency to enhance or reduce the liquid flow turbulence intensity as indicated by Serizawa and Kataoka (1990). In the case of enhanced turbulence, as depicted in Fig. 4b, the liquid velocity profile at the core is flattened by the additional turbulence while having a relatively steep decrease almost mimicking a step change close to the pipe wall. The recorded liquid velocity at the wall is not zero thereby exposing some

uncertainties of the experiment (Politano et al., 2003). Nevertheless, the predicted velocity profiles, particularly the sharp decrease of the decreasing velocities close to wall, were successfully captured by all models and compared reasonably well with measurements. The MUSIG model appeared to yield marginally better agreement than the other models. One possible reason could be the higher resolution of bubble classes adopted within the MUSIG model. By introducing multiple size groups to discretize the range of bubble sizes that could exist within the flow, instead of using a single average parameter in the ABND model, the Sauter mean bubble diameter could have been better resolved that eventually enhanced the prediction of the liquid velocities. This issue will become more apparent by comparing the predictions of Sauter mean bubble diameter against measurements which will be presented in later sections.

5.2 *Experimental data of Hibiki et al. (2001)*

Although encouraging results were obtained and discussed in the previous section, unfortunately, Liu and Bankoff (1993a, 1993b) did not report other primitive variable measurements for the two flow conditions, such as: Interfacial Area concentration (IAC), Sauter mean bubble diameter and gas time-averaged velocity. A closer examination of the hydraulic dynamic behaviour of the isothermal bubbly flows can be analysed by further comparing the model predictions with a more comprehensive experimental data reported by Hibiki et al. (2001). Details of the comparison are discussed below.

5.2.1 *Void fraction distribution*

Fig. 5 compares the gas void fraction profiles obtained from the ABND and MUSIG models with the measured data in four different bubbly flow conditions. In low void fraction cases (i.e. $\langle j_f \rangle = 0.491$ m/s), wall peaking profiles were well established at

the first measuring station of $z/D=6.0$ due to the considerably low liquid and gas velocities. However, the radial void fraction profile subsequently evolved along the axial direction becoming a well-developed wall peaking at the location of $z/D=53.5$ for $\langle j_f \rangle = 0.986 \text{ m/s}$. As depicted, the phenomenological evolution of the wall peaking behaviours was properly captured by the ABND and MUSIG models.

For $\langle j_f \rangle = 0.491 \text{ m/s}$ and $\langle j_g \rangle = 0.0556 \text{ m/s}$, void fractions close to the pipe wall were slightly under-predicted by the ABND models at the location of $z/D=53.5$ (see also in Fig. 5f). Similar discrepancies were also found in Fig. 5g and Fig. 5h. In contrast, the wall peak values were better predicted by the MUSIG. This could be resulted from the superior predictions of bubble diameter which will be discussed in more detail in the next section. Nonetheless, the results revealed that the MUSIG has a tendency to predict higher void fraction at the core of pipe. Again, this could be attributed to the uncertainties embraced in the adopted turbulence and wall lubrication models. Overall, all the model predictions of the void fraction profile at the two measuring locations were in satisfactory agreement with measurements.

5.2.2 Sauter mean bubble diameter

Fig. 6 illustrates the predicted and measured Sauter mean bubble diameter distributions at two measuring stations, corresponding to that of void fraction profiles in Fig. 5. As measured by Hibiki et al. (2001), the Sauter mean bubble diameter profiles were almost uniform along the radial direction with some increase in size at the vicinity of the wall. The slightly larger bubbles were formed near the wall might be due to the tendency of small bubbles migrating towards the wall creating higher concentration of bubbles thereby increasing the likelihood of possible bubble coalescence. In general, predictions from all models agreed reasonably well with the measurements. For all the

flow cases and locations especially for the MUSIG, predictions of the model were in remarkable agreement with the measurement and were also obviously superior than other ABND models.

The above results clearly demonstrated that population balance of bubbles was accurately captured by using the “Multiple Size Groups” approach. Compared to the single average parameter of ABND models, higher resolution of multiple size groups were found to be better resolved through the dynamical changes of bubbles size distribution. Since the Sauter mean bubble diameter is generally closely coupled with the interfacial momentum forces (i.e. drag and lift forces), better predictions of the bubble diameter could significantly improve the prediction of liquid and gas velocities (see also in section 5.2.4). Unfortunately, as extra transport equations were required in the numerical calculations, additional computational effort is required to solve these equations. Computational efficiency and accuracy are issues of on-going debate. In the present study, the MUSIG model required around twice of the computational effort than the ABND models under the same arrangement of computational resources.

5.2.3 Interfacial Area Concentration (IAC)

Based on the assumption where the bubbles are spherical, the local Interfacial Area Concentration (IAC) profiles can be related to the local void fraction and Sauter mean bubble diameter according to $a_{if} = 6\alpha_g / D_s$. The measured and predicted local interfacial area concentration profiles for the respective two axial locations are shown in Fig. 7. The IAC radial profiles roughly followed the same trend of the void fraction distribution as stipulated in Fig. 5. Similar to the comparison for the void fraction distribution, predictions of all models at the two measuring stations were in satisfactory agreement with measurements. The difference between predicted and measured data could be attributed to the deviation of bubble shape from sphere. Especially in high gas

void fraction cases, large distorted bubbles start to emerge introducing errors in IAC prediction. The peak values of IAC close to wall were, however, better predicted by the MUSIG model. This could have been benefited from the accurate prediction of the Sauter mean bubble diameter and void fraction values. In Fig. 7f-h, the IAC was over-predicted at the core region as reflected by both models. Nevertheless, the predictions of MUSIG generally appeared to yield marginally better agreement than the ABND models.

5.2.4 Time-averaged liquid and gas velocities

Fig. 8 shows the local radial gas and liquid velocity distributions at the measuring station of $z/D=53.5$ close to the outlet of the pipe. For low liquid superficial velocity cases (i.e. $\langle j_f \rangle = 0.491 \text{ m/s}$), except the simulation results shown in Fig. 8f, all ABND models predictions of the gas and liquid velocity compared favourably with the experimental data. Owing to the errors introduced through the bubble diameter predictions, liquid velocities at the core of the pipe were generally under-predicted at the location of $z/D=53.5$ (see also in Fig. 8f). Similar observations were also found for the predictions of the gas or liquid velocity for $\langle j_f \rangle = 0.986 \text{ m/s}$ shown in Fig. 8c-d and Fig. 8g-h.

Conversely, predictions made by the MUSIG model as depicted in Fig. 8a-d compared very well with measurements and were found to be noticeably better than those of ABND models. Although the liquid velocities at the core were still under-predicted for $\langle j_f \rangle = 0.986 \text{ m/s}$, the MUSIG model generally gave better agreement than the ABND models. The ability to better determine the Sauter mean bubble diameter could indirectly enhance the liquid velocity predictions by the provision of a

more appropriate description of the interfacial forces within the interfacial momentum transfer between the air and water phases.

5.3 Examination of limitations of the population balance approaches

The superior performance of the MUSIG model as well as encouraging predictions made by the ABND models clearly demonstrated their viable applications in resolving the coalescence and breakage bubble mechanistic behaviours in isothermal bubbly flow conditions. Nevertheless, the flow cases that have been investigated from above generally possessed only weak bubble-bubble interactions and narrow bubble size distributions. Attention is now directed in assessing whether the two population balance approaches can be applied beyond the bubbly flow regime.

Two transitional flow conditions: $\langle j_f \rangle = 0.491$ m/s, $\langle j_g \rangle = 0.129$ m/s and $\langle j_f \rangle = 0.986$ m/s, $\langle j_g \rangle = 0.242$ m/s, are investigated. Similar to the bubbly flow simulations as aforementioned, the measured and predicted local radical void fraction, Sauter mean bubble diameter, IAC and gas velocity distribution at the measuring station of $z/D=53.5$ for the two flow conditions are depicted in Fig. 9. Notable discrepancies can be observed when comparing the numerical results against the experimental measurements. Wall peaking values of void fraction and IAC were considerably under-predicted by all the models. Particularly, Yao and Morel (2004) model substantially over-predicted the Sauter mean bubble diameter in the two flow conditions. Consequentially, the over-estimation of the bubble size introduced significant error in the void fraction, IAC and gas velocity predictions.

Considering the MUSIG model, it did not fare much better than the ABND model even though higher resolution could be imposed within the model to account for the different ranges of bubble sizes. At the core region, local distributions of void fraction

and IAC were grossly over-predicted. This could be possibly due to inadequacy of the coalescence and breakage mechanisms that have been based on spherical-shape assumption is invalid for bubbles beginning to markedly distort or become cap-shape bubbles within the transitional flow regime. As suggested by the recent phenomenological investigation by Ho and Yeoh (2005), the coalescence and breakage rates based on the formulation for spherical bubbles introduced significant error into the calculations for these flow conditions. The Sauter mean bubble diameter was grossly over-predicted while the gas velocity profile was considerably under-predicted. It was apparent that the assumption using spherical-shape bubbles to model distorted bubble interactions was not strictly appropriate in simulating bubbly-to-slug transition flows. The likelihood of coalescence and breakage mechanisms other than driven by random collision and turbulent shearing needs to be further investigated. Moreover, the assumption of finely dispersed of bubbles could be another plausible source of error where in high void fraction condition, bubbles become closely packed and their movements are thus affected by the neighbouring bubbles, which requires more investigations.

6 Conclusions

An averaged one-group population balance approach, the Average Bubble Number Density (ABND) transport equation, coupled with the Eulerian-Eulerian two-fluid model is presented in this paper to handle the gas-liquid bubbly flows under isothermal conditions. Three forms of the ABND model incorporating three coalescence and breakage mechanisms by Wu et al. (1998), Hibiki and Ishii (2002) and Yao and Morel (2004) were compared against the MUSIG model and two experimental data by Liu and Bankoff (1993a,b) and Hibiki et al. (2001). Interfacial momentum transfer that accommodated various interfacial force including drag, lift, wall lubrication and

turbulent dispersion force was also accounted. In general, both population balance approaches gave close agreement for the local radial distributions of void fraction, interfacial area concentration, Sauter mean bubble diameter and gas and liquid velocities against measurements. With the MUSIG model, predictions of bubble diameter attained remarkable agreement with the measurements and obviously superior than ABND models because of the higher resolution imposed on the bubble size distribution. As a result, predictions for the gas and liquid velocity of MUSIG model were also notably better than those of ABND models. Numerical results clearly showed that the range of bubbles sizes exists in the gas-liquid flows required substantial resolution and they were achieved through the “Multiple Size Groups” approach. In the present study, the computations using the MUSIG model was twice as slow when the ABND was applied under the same computational resources. Nonetheless, predictions of ABND models were found to yield satisfactory agreement with measurements though appearing marginally inferior to some degree to the MUSIG model results. The ABND models thus can be considered as a viable option for a rapid design tool in simulating bubbly flows with reasonable accuracy. For the case of acquiring highly accurate Sauter mean bubble diameter distribution, the MUSIG model serves as the best alternative in handling such flows.

In examining the limitations of both models, simulations for transition flow regime (i.e. high void fraction condition) were also investigated. Notable discrepancies were found between the numerical and experimental results. Wall peaking values of void fraction and IAC were considerably under-predicted by both models. The reason of these discrepancies could be due to the departure from the ideal spherical-shape consideration to distorted cap-shape bubbles. This inappropriate assumption to modelling distorted compared with spherical bubbles interactions introduced significant

error into the calculations. This shortcoming could be overcome by possibly enhancing the coalescence and breakage mechanisms to include distorted bubble-bubble interactions. Conceptually, the one-group approach based on spherical bubbles could be extended to two-group approach that distinguishes the “small” spherical bubbles from the “large” distorted bubbles (Hibiki and Ishii, 2000b; Fu and Ishii, 2002a,b). Also, considerable efforts have been devoted in developing an inhomogeneous MUSIG model using different momentum equations to describe individual velocity of each bubble size group (Frank et al., 2005). One possible future development is to further formulate the inhomogeneous model with the two-group approach. Furthermore, the recent model proposal using least square method (LSM) for solving PBEs appears to be an innovative approach for bubbly flow modelling (Dorao and Jakobsen, 2006, 2007).

Finally, as bubbles become closely packed in high void fraction conditions and their movements greatly hindered by the neighbouring bubbles, adequate coalescence and breakage rates and the interfacial forces based on finely dispersed bubbles need to be formulated and incorporated within the models.

Acknowledgment

The financial support provided by the Australian Research Council (ARC project ID DP0556095) is gratefully acknowledged.

References

- ANSYS, (2005). CFX-10 User Manual. ANSYS CFX.
- Antal, S.P., Lahey Jr., R.T., Flaherty, J.E., (1991). Analysis of phase distribution in fully developed laminar bubbly two-phase flow. *Int. J. Multiphase Flow*, 17, 635-652.
- Bertola, F., Grundseth, J., Hagesaether, L., Dorao, C., Luo, H., Hjarbo, K.W., Svendsen, H.F., Vanni, M.B. Jakobsen, H.A., (2003). Numerical analysis and experimental validation of bubble size distributions in two phase bubble column reactors, in: *Proceedings of the 3rd European-Japanese Two Phase Flow Group Meeting*, Certosa di Pontignano.

- Bove, S., Solberg, T., Hjertager, B.H., (2005). A novel algorithm for solving population balance equations: the parallel parent and daughter classes. Derivation, analysis and testing. *Chem. Eng. Sci.*, 60, 1449-1464.
- Bukur, D.B., Daly, J.G., Patel, S.A., (1996). Application of γ -ray attenuation for measurement of gas hold-ups and flow regime transitions in bubble columns. *Indust. & Eng. Chem. Res.*, 35, 70-80.
- Burns, A.D., Frank, T., Hamill, I., Shi, J., (2004). The Farve averaged drag model for turbulent dispersion in Eulerian Multi-phase flows, in: *Proceeding of the Fifth International Conference on Multiphase flow*, Yokohama, Japan.
- Chen, P., Sanyal, J., Duduković, M.P., (2005). Numerical simulation of bubble columns flows: effect of different breakup and coalescence closures. *Chem. Eng. Sci.*, 60, 1085-1101.
- Chesters, A.K., Hoffman, G., (1982) Bubble coalescence in pure liquids, *Appl. Sci. Res.*, 38, 353-361.
- Cheung, S.C.P., Yeoh, G.H., Tu, J.Y., (2006). On the modelling of population balance in isothermal vertical bubbly flows – average bubble number density approach. *Chem. Eng. Process.*, in Press.
- Coulaloglou, C.A., Tavlarides, L.L., (1977). Description of interaction processes in agitated liquid-liquid dispersions. *Chem. Eng. Sci.*, 32, 1289.
- Drew, D.A., Lahey Jr., R.T., (1979). Application of general constitutive principles to the derivation of multidimensional two-phase flow equation. *Int. J. Multiphase Flow*, 5, 243-264.
- Dorao, C.A., Jakobsen, H.A., (2006). A least squares method for the solution of population balance problems. *Computer and Chemical Engineering*, 30, 535-547.
- Dorao, C.A., Jakobsen, H.A., (2007). Time-space-property least square spectral method for population balance problems. *Chem. Eng. Sci.*, 62, 1323-1333.
- Frank, T., Shi, J., Burns, A.D., (2004). Validation of Eulerian multiphase flow models for nuclear safety application, in: *Proceeding of the Third International Symposium on Two-Phase Modelling and Experimentation*, Pisa, Italy.
- Frank, T., Zwart, P.J., Shi, J., Krepper, E., Lucas, D., Rohde, U., (2005). Inhomogeneous MUSIG model – a population balance approach for polydispersed bubbly flow, in: *Proceeding of International Conference for Nuclear Energy for New Europe*, Bled, Slovenia.
- Fu, X.Y., Ishii, M., (2002a). Two-group interfacial area transport in vertical air-water flow I. Mechanistic model. *Nuclear Eng. & Des.*, 219, 143-168.
- Fu, X.Y., Ishii, M., (2002b). Two-group interfacial area transport in vertical air-water flow II. Model evaluation. *Nuclear Eng. & Des.*, 219, 169-190.
- George, D.L., Shollenberger, K.A., Torczynski, J.R., (2000). Sparger effect on gas volume fraction distributions in vertical bubble-column flows as measured by gamma-densitometry tomography, in: *ASME 2000 Fluid Engineering Division Summer Meeting*, Boston, USA.

- Hibiki, T., Ishii, M., (2000a). One-group interfacial area transport of bubbly flows in vertical round tubes. *Int. J. Heat Mass Trans.*, 43, 2711-2726.
- Hibiki, T., Ishii, M., (2000b). Two-group interfacial area transport equations at bubbly-to-slug flow transition. *Nuclear Eng. & Des.*, 202, 39-76.
- Hibiki, T., Ishii, M., (2002). Development of one-group interfacial area transport equation in bubbly flow systems. *Int. J. Heat Mass Trans.*, 45, 2351-2372.
- Hibiki, T., Ishii, M., Xiao, Z., (2001). Axial interfacial area transport of vertical bubble flows. *Int. J. Heat Mass Trans.*, 44, 1869-1888.
- Ho, M.K., Yeoh, G.H., (2005). Phenomenological investigation of gas-liquid flows. *Trans. American Nucl. Soci.*, 93, 408-409.
- Ishii, M. (1975). *Thermo-fluid dynamic theory of two-phase flow*. Eyrolles, Paris.
- Ishii, M., Zuber, N., (1979). Drag coefficient and relative velocity in bubbly, droplet or particulate flows. *A.I.Ch.E. Journal*, 5, 843-855.
- Kocamustafaogullari, G., Ishii, M., (1995). Foundation of the interfacial area transport equation and its closure relations. *Int. J. Heat Mass Trans.*, 38, 481-493.
- Krepper, E., Lucas, D., Prasser, H., (2005). On the modelling of bubbly flow in vertical pipes. *Nucl. Eng. Des.*, 235, 597-611.
- Kumar, S., Ramkrishna, D., (1996a). On the solution of population balance equations by discretisation – I. A fixed pivot technique. *Chem. Eng. Sci.*, 51, 1311-1332.
- Kumar, S., Ramkrishna, D., (1996b). On the solution of population balance equations by discretisation – II. A moving pivot technique. *Chem. Eng. Sci.*, 51, 1333-1342.
- Levich, V.G. (1962). *Physicochemical Hydrodynamics*. Prentice-Hall, Englewood Cliffs, NJ, USA.
- Liu, T.J., Bankoff, S.G., (1993a). Structure of air-water bubbly flow in a vertical pipe – I. Liquid mean velocity and turbulence measurements. *Int. J. Heat Mass Trans.*, 36, 1049-1060.
- Liu, T.J., Bankoff, S.G., (1993b). Structure of air-water bubbly flow in a vertical pipe – II. Void fraction, bubble velocity and bubble size distribution. *Int. J. Heat Mass Trans.*, 36, 1061-1072.
- Luo, H., Svendsen, H., (1996). Theoretical model for drop and bubble break-up in turbulent dispersions. *A.I.Ch.E Journal*, 42, 1225-1233.
- Marchisio, D.L., Fox, P.O., (2005). Solution of population balance equations using the direct quadrature method of moments. *J. of Aero. Sci.*, 36, 43-73.
- Marchisio, D.L., Vigil, R.D., Fox, R.O., (2003a). Quadrature method of moments for aggregation-breakage processes. *J. of Colloid. & Inter. Sci.*, 258, 322-334.
- Marchisio, D.L., Pikturna, J.T., Fox, R.O., Vigil, R.D., (2003b). Quadrature method for moments for population-balance equations. *A.I.Ch.E. J.*, 49, 1266-1276.

- Menter, F.R. (1994). Two-equation eddy viscosity turbulence models for engineering applications. *AIAA J.*, 32, 1598-1605.
- Olmos, E., Gentric, C., Vial, Ch., Wild, G., Midoux, N., (2001). Numerical simulation of multiphase flow in bubble column. Influence of bubble coalescence and break-up. *Chem. Eng. Sci.*, 56, 6359-6365.
- Oolman, T., Blanch, H.W., (1986a). Bubble coalescence in air-sparged bioreactor. *Biotechnol. Bioeng.*, 28, 578-584.
- Oolman, T., Blanch, H.W., (1986b). Bubble coalescence stagnant liquids. *Chem. Eng. Commun.*, 43, 237-261.
- Pohorecki, R., Moniuk, W., Bielski, P., Zdrojkowski, A., (2001). Modelling of the coalescence/redispersion processes in bubble columns. *Chem. Eng. Sci.*, 56, 6157-6164.
- Politano, M.S., Carrica, P.M., Converti, J., (2003). A model for turbulent polydisperse two-phase flow in vertical channels. *Int. J. Multiphase Flow*, 29, 1153-1182.
- Prince, M.J., Blanch, H.W., (1990). Bubble coalescence and break-up in air sparged bubble columns. *A.I.Ch.E Journal*, 36, 1485-1499.
- Ramkrishna, D. (2000). *Population balance*, Academic Press, San Diego.
- Ramkrishna, D., Mahoney, A.W., (2002). Population balance modeling. Promise for the future. *Chem. Eng. Sci.*, 57, 595-606.
- Rotta, J.C. (1972). *Turbulente Stromungen*, Teubner B.G., Stuttgart, 1972.
- Sato, Y., Sadatomi, M., Sekoguchi, K., (1981). Momentum and heat transfer in two-phase bubbly flow – I. *Int. J. of Multiphase Flow*, 7, 167-178.
- Serizawa, A., Kataoka, I., (1988). Phase distribution in two-phase flow, in: Afgan, N.H. ed., *Transient phenomena in multiphase flow*. Washington, DC, 179-224.
- Serizawa, A., Kataoka, I., (1990). Turbulence suppression in bubbly two-phase flow. *Nucl. Eng. Des.*, 122, 1-16.
- Sevik, M., Park, S.H., (1973). The splitting of drops and bubbles by turbulent fluid flow. *J. Fluid Eng., Trans. ASME*, 95, 53-60.
- Taitel, Y., Bornea, D., Dukler, E.A., (1980). Modelling flow pattern transition for steady upward gas-liquid flow in vertical tubes. *A.I.Ch.E. Journal*, 26, 345-354.
- Tomiya, A. (1998). Struggle with computational bubble dynamics, in: *Proceeding of the Third International Conference on Multiphase Flow*. Lyon, France.
- Wellek, R.M., Agrawal, A.K., Skelland, A.H.P., (1966). Shapes of liquid drops moving in liquid media. *A.I.Ch.E. Journal*, 12, 854.
- Wu, Q., Kim, S., Ishii, M., Beus, S.G., (1998). One-group interfacial area transport in vertical bubbly flow. *Int. J. Heat Mass Trans.*, 41, 1103-1112.
- Yao, W., Morel, C., (2004). Volumetric interfacial area prediction in upwards bubbly two-phase flow. *Int. J. Heat Mass Trans.*, 47, 307-328.

- Yeoh, G.H., Tu, J.Y., (2004). Population balance modelling for bubbly flows with heat and mass transfer. *Chem. Eng. Sci.*, 59, 3125-3139.
- Yeoh, G.H., Tu, J.Y., (2005). Thermal-hydrodynamic modelling of bubbly flows with heat and mass transfer. *A.I.Ch.E. J.*, 51, 8-27.
- Yeoh, G.H., Tu, J.Y., (2006). Numerical modelling of bubbly flows with and without heat and mass transfer. *App. Math. Model.* 30, 1067-1095.

List of Table Captions

Table 1 Bubbly flow conditions and its inlet boundary conditions employed in the present study

Table 2 Details of numerical meshes adopted for the grid sensitivity study

Table 3 Diameter of each discrete bubble class for MUSIG model

Table 1

Superficial liquid velocity, $\langle j_f \rangle$ (m/s)	Superficial gas velocity, $\langle j_g \rangle$ (m/s)		
<i>Liu and Bankoff (1993a) experiment</i>	Bubbly flow Regime	Transition Regime	
1.087	0.0270	0.1120	
$[\alpha_g]_{z/D=0.0}$ (%)	[2.5]	[10.0]	
$[D_s]_{z/D=0.0}$ (mm)	[3.0]	[3.0]	
<i>Hibiki et al. (2001) experiment</i>			
0.491	0.0275	0.0556	0.129
$[\alpha_g]_{z/D=0.0}$ (%)	[5.0]	[10.0]	[20.0]
$[D_s]_{z/D=0.0}$ (mm)	[2.5]	[2.5]	[2.5]
0.986	0.0473	0.1130	0.242
$[\alpha_g]_{z/D=0.0}$ (%)	[5.0]	[10.0]	[20.0]
$[D_s]_{z/D=0.0}$ (mm)	[2.5]	[2.5]	[2.5]

Table 2

	Liu and Bankoff (1993a) experiment		Hibiki et al. (2001) experiment	
	$L \times W \times H$	Total	$L \times W \times H$	Total
<i>Coarse</i>	10×10×40	4,000	10×10×40	4,000
<i>Medium</i>	20×20×40	16,000	26×26×80	54,080
<i>Fine</i>	24×24×120	69,120	30×30×120	108,000

Table 3

Class No.	Central class diameter, d_i (mm)
1	0.5
2	1.5
3	2.5
4	3.5
5	4.5
6	5.5
7	6.5
8	7.5
9	8.5
10	9.5

List of Figure Captions

- Fig. 1 Map of flow regime and the bubbly flow conditions studied in the present study.
- Fig. 2 Visualization and mesh distribution of computational models of: (a) Liu and Bankoff (1993a) experiment and (b) Hibiki et al. (2001) experiment.
- Fig. 3 Predicted radial void fraction distribution at $z/D = 36.0$ and experimental data of Liu and Bankoff (1993b).
- Fig. 4 Predicted radial liquid velocity profile at $z/D = 36.0$ and experimental data of Liu and Bankoff (1993a).
- Fig. 5 Predicted radial void fraction distribution and experimental data of Hibiki et al. (2001): (a-d) $z/D = 6.0$ and (e-h) $z/D = 53.5$.
- Fig. 6 Predicted Sauter mean bubble diameter distribution and experimental data of Hibiki et al. (2001): (a-d) $z/D = 6.0$ and (e-h) $z/D = 53.5$.
- Fig. 7 Predicted Interfacial Area Concentration (IAC) distribution and experimental data of Hibiki et al. (2001): (a-d) $z/D = 6.0$ and (e-h) $z/D = 53.5$.
- Fig. 8 Predicted radial gas and liquid velocity profile and experimental data of Hibiki et al. (2001) at $z/D = 53.5$: (a-d) for gas velocity and (e-h) for liquid velocity.
- Fig. 9 Predicted and measured local radial void fraction, Sauter mean bubble diameter, IAC and liquid velocity distribution at $z/D = 53.5$.

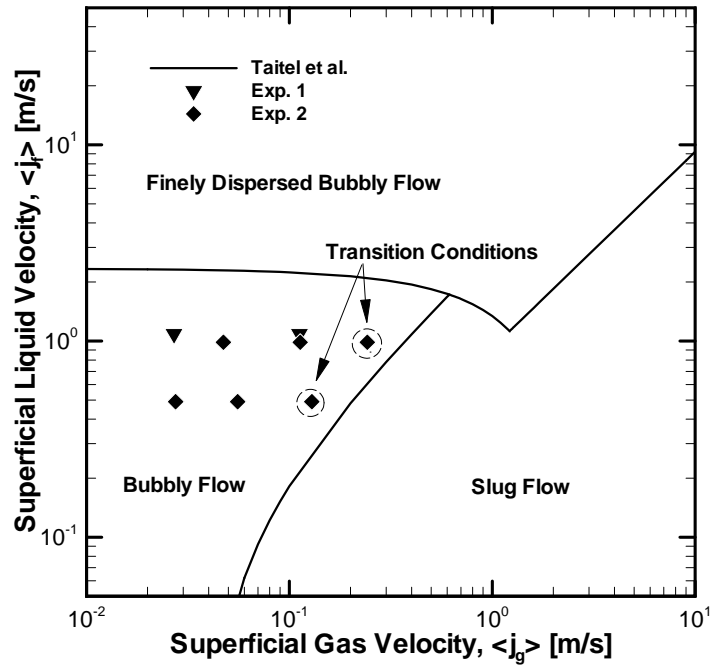


Fig. 1

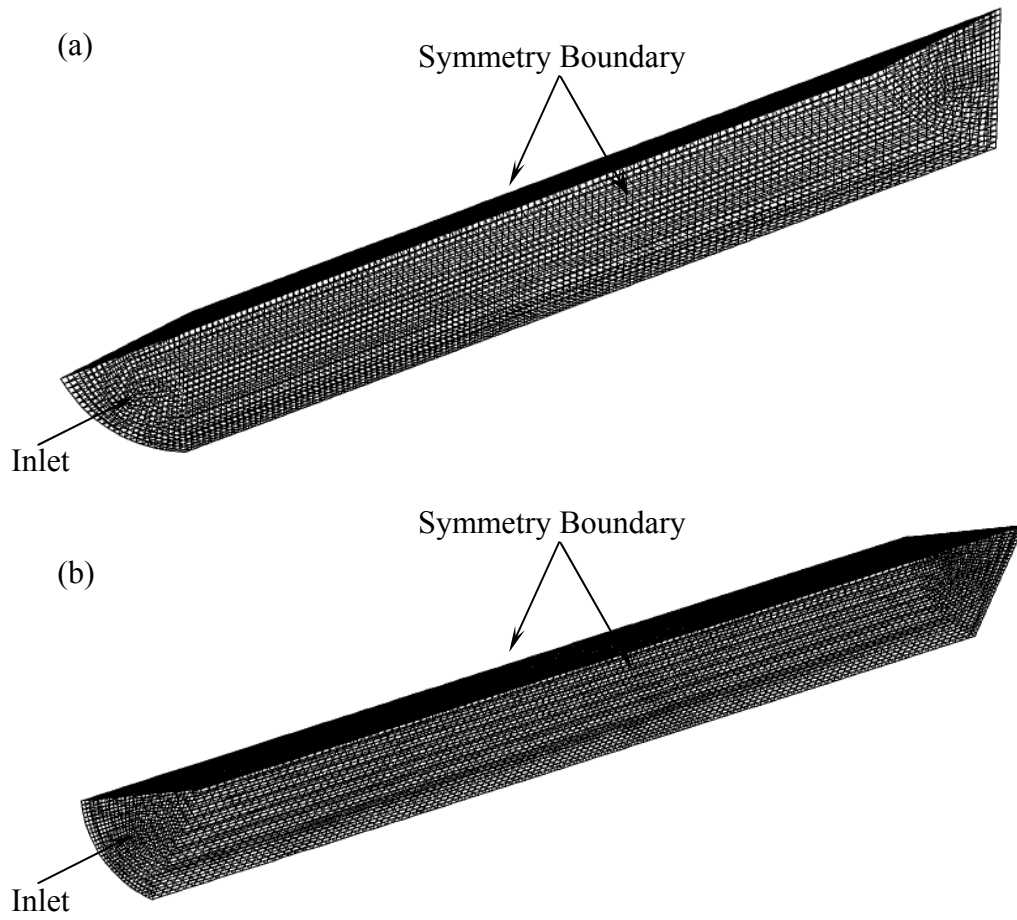


Fig. 2

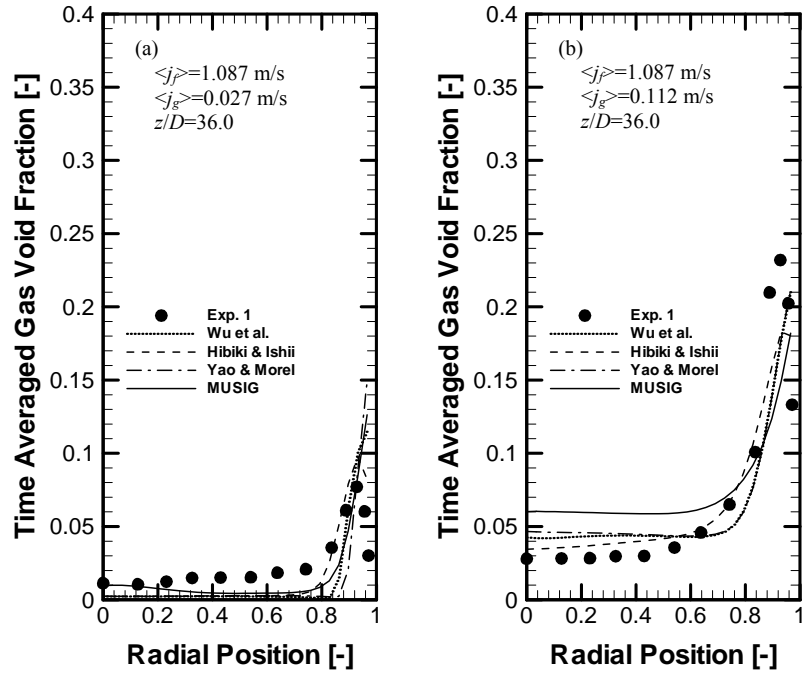


Fig. 3

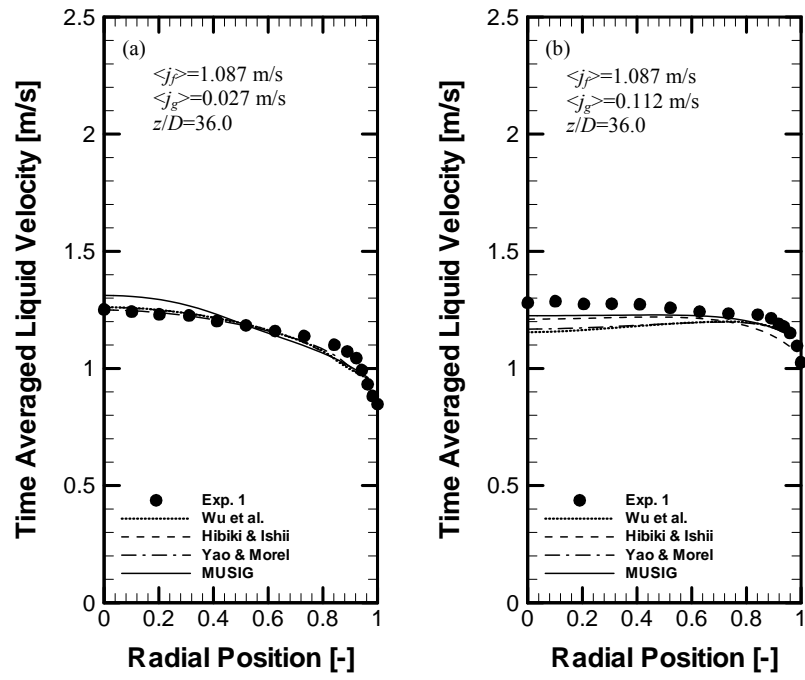


Fig. 4

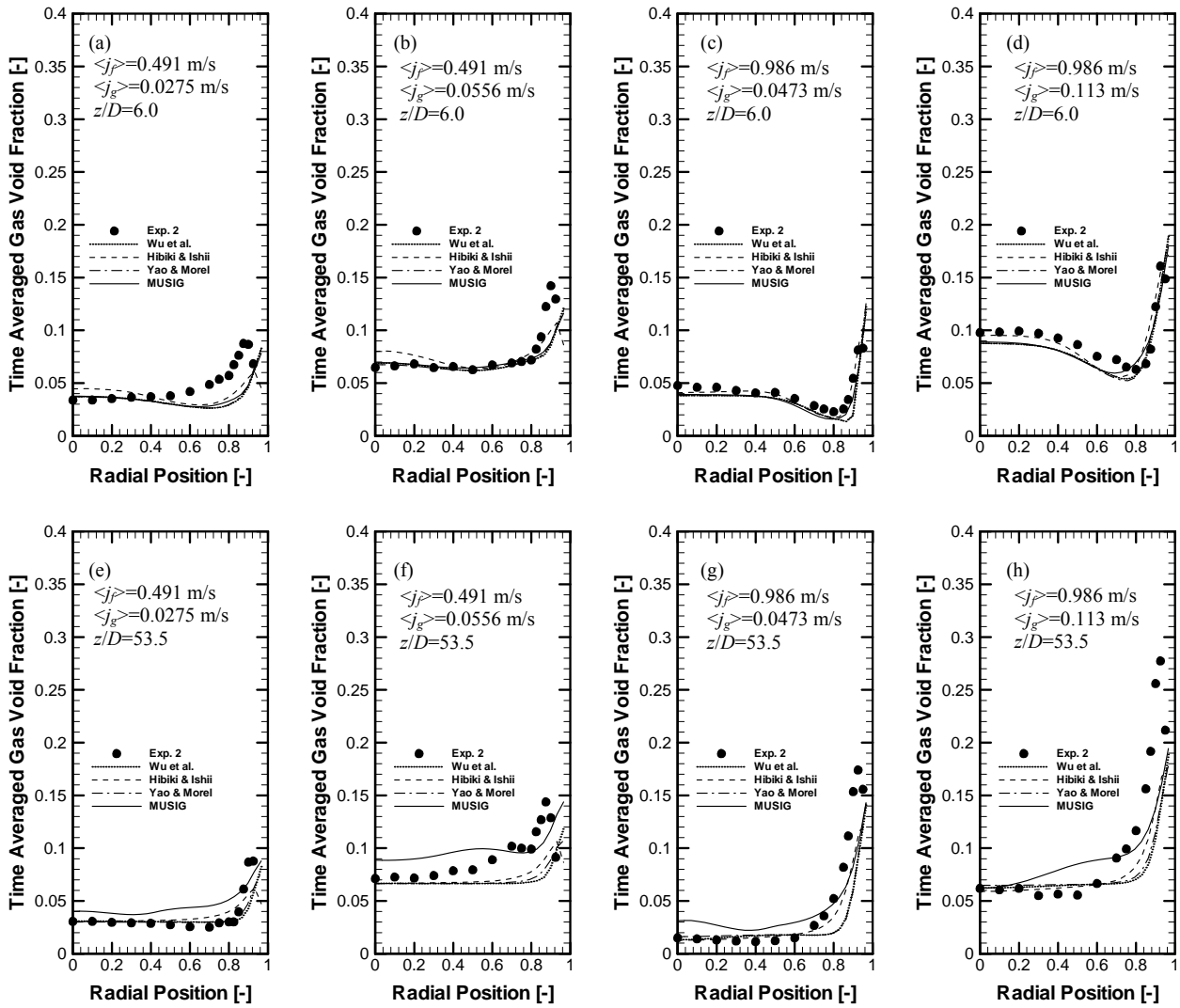


Fig. 5

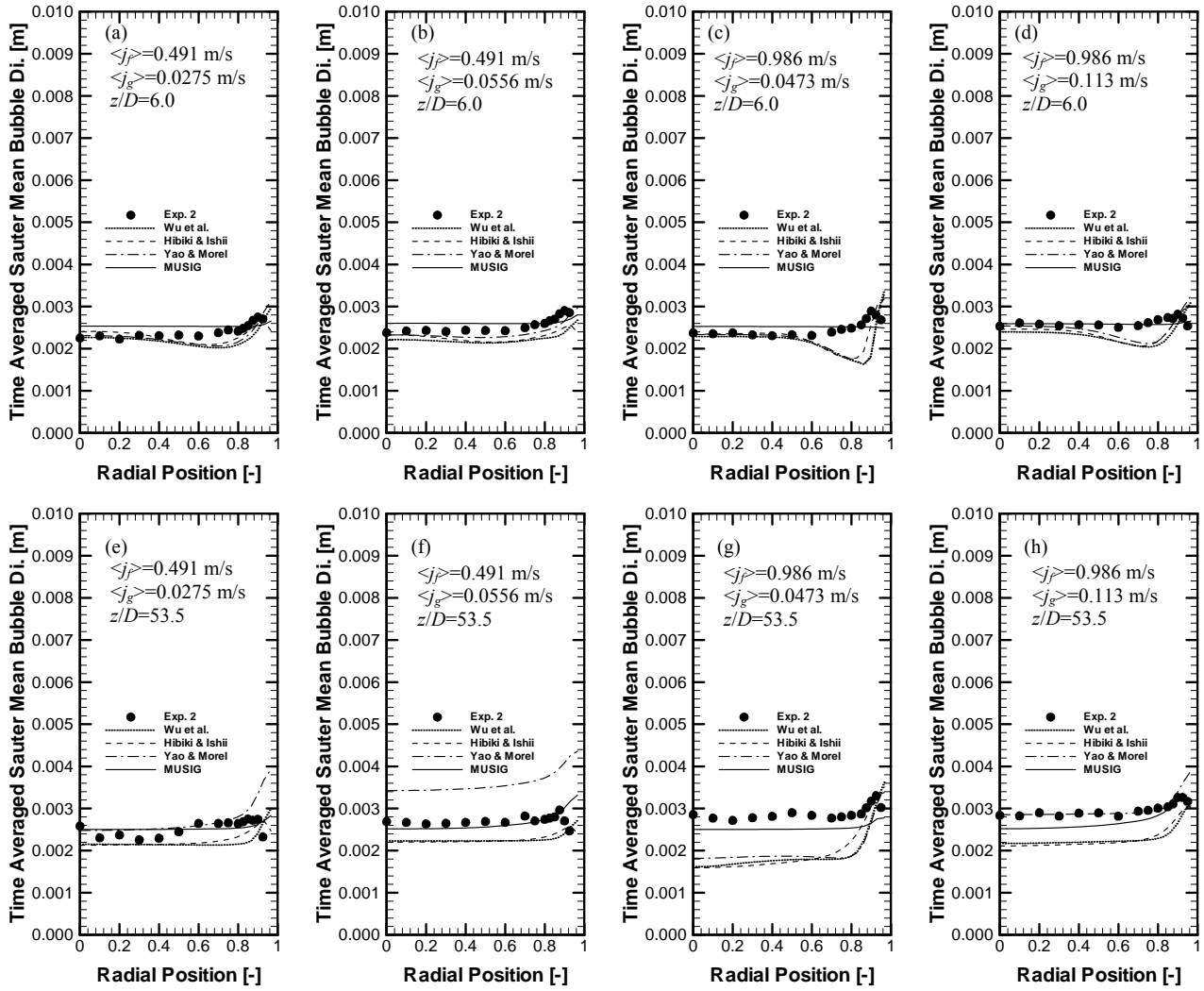


Fig. 6

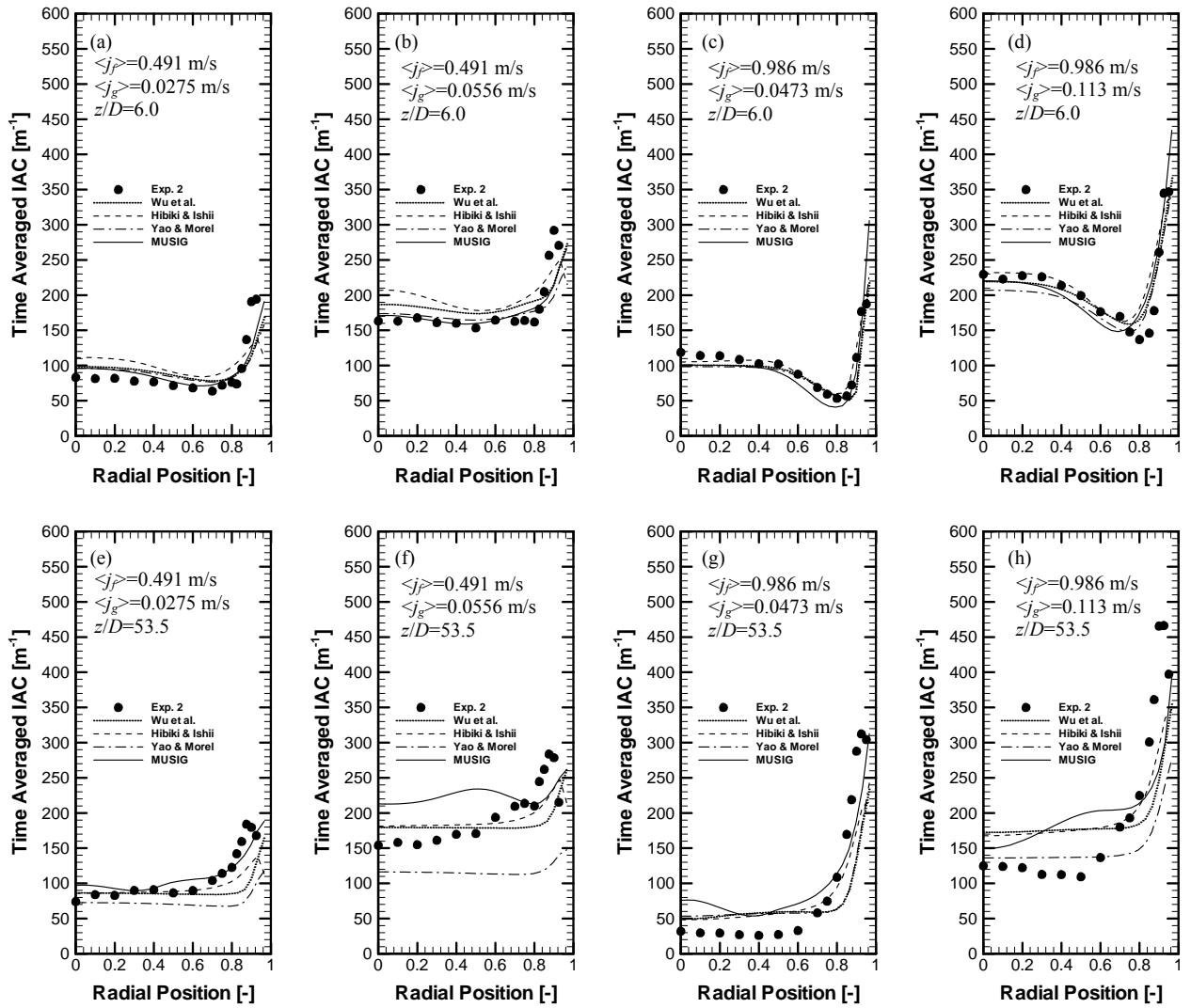


Fig. 7

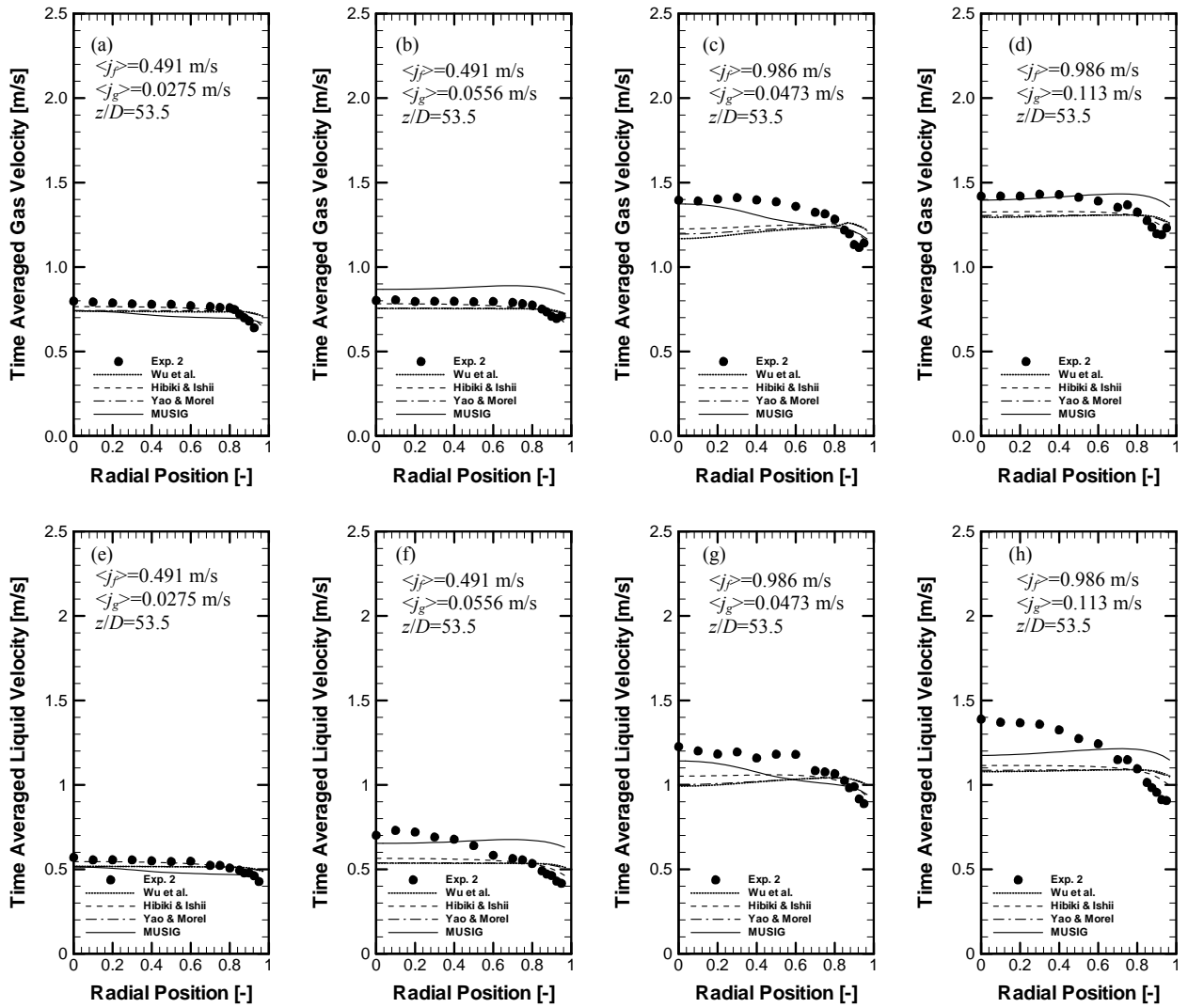


Fig. 8

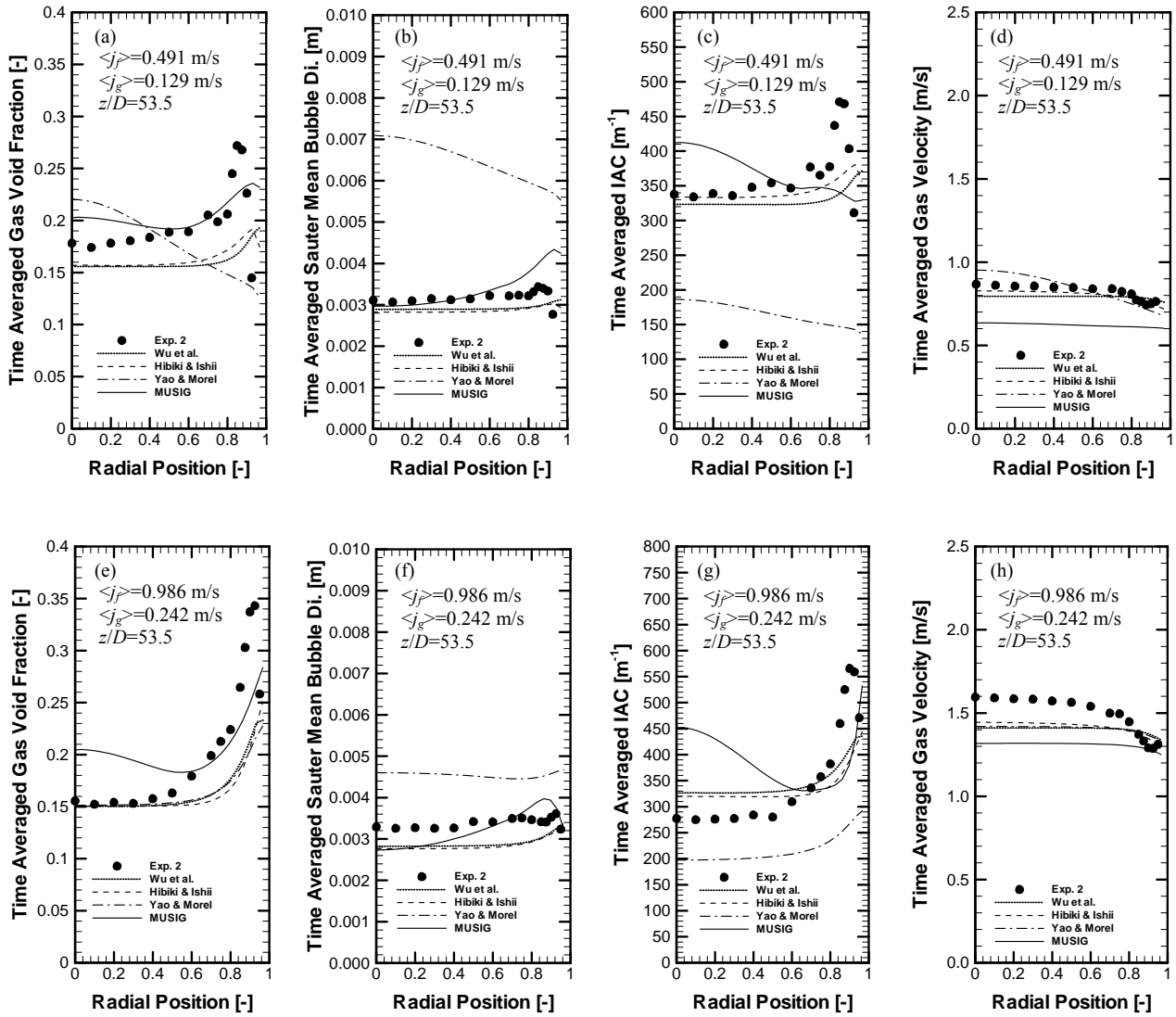


Fig. 9